Available online at www.sciencedirect.com
ScienceDirect
Ceramics International 36 (2010) 473–482
CERAMICS INTERNATIONAL
www.elsevier.com/locate/ceramint

Influence of processing route on microstructure and mechanical properties of $MgAl_2O_4$ spinel

Ibram Ganesh [a,*], G. Jaganatha Reddy [a], G. Sundararajan [a], Susana M. Olhero [b], Paula M.C. Torres [c], José M.F. Ferreira [c]

[a] *Centre for Advanced Ceramics, International Advanced Research Centre for Powder Metallurgy and New Materials (ARCI), Hyderabad 500 005, AP, India*
[b] *Department of Mechanical Engineering and Industrial Management, FEUP, University of Porto, Porto, Portugal*
[c] *Department of Ceramics and Glass Engineering, CICECO, University of Aveiro, Aveiro P-3810193, Portugal*

Received 7 May 2009; received in revised form 30 July 2009; accepted 24 August 2009
Available online 22 September 2009

Abstract

This paper reports on process dependant microstructural and mechanical properties of $MgAl_2O_4$ spinel (MAS) ceramics. Two MAS powders with different chemical compositions were synthesized by solid-state reaction of alumina and calcined caustic magnesia at 1400 °C for 1 h. The surface of the as obtained MAS powders was passivated against hydrolysis by coating it with H_3PO_4 and $Al(H_2PO_4)_3$ species dissolved in ethanol at 80 °C for 24 h. The as protected powders could then be dispersed in aqueous solutions of tetramethylammonium hydroxide (TMAH) and Duramax D-3005 as dispersing agents to obtain stable slurries with 45 vol.% solids loading. The stable aqueous MAS slurries were consolidated by slip casting (SC), gelcasting (GC), hydrolysis assisted solidification (HAS) and hydrolysis induced aqueous gelcasting (GCHAS) routes, fully dried and then sintered for 1 h at 1650 °C. For comparison purposes, dense MAS ceramics were also prepared following a conventional dry-powder pressing (DP) and temperature induced gelation (TIG) routes. All the sintered MAS ceramics were thoroughly characterized for bulk density, apparent porosity, water absorption capacity, SEM microstructure, XRD phase, hardness, 3-point bend strength, and percentage of shrinkage to evaluate the suitability of the processing routes for fabricating defect free components with near-net shape. Among the various techniques employed, the GCHAS was found to be best for fabricating near-net shape MAS ceramics.

Keywords: A. Slip casting; C. Mechanical properties; $MgAl_2O_4$ spinel; Gelcasting; Hydrolysis assisted solidification; Hydrolysis induced aqueous gelcasting

1. Introduction

Recently, magnesium aluminate ($MgAl_2O_4$) spinel (MAS) has received a great deal of attention as a technologically important material [1–12]. It has been employed in several applications such as, optical windows for pressure vessels and bullet proof vehicles [1–3], alternative materials to replace the conventional carbon anode in aluminium electrolytic cells [4], humidity sensors [5], and refractory materials for cement rotary kilns and steel ladles [6,7] owing to its important properties such as high melting point (2135 °C), high hardness (16 GPa), relatively low density (3.58 g/cm^3), excellent transmittance in the range of 0.25–5.0 μm wavelength, high strength at room and at elevated temperature (180 MPa), high chemical inertness, relatively low thermal expansion coefficient (9×10^{-6} °C^{-1} between 30 and 1400 °C), high thermal shock resistance, etc. [8–12]. Furthermore, MAS does not react with SiO_2 until 1735 °C, with MgO or CaO until 2000 °C, with Al_2O_3 until 1925 °C [12]. In spite of the above mentioned advantages, the formation of MAS by solid-state reaction is associated with a severe volume expansion (~8%) that hinders full dense MAS ceramics to be achieved in a single-stage-firing process [13]. In order to overcome the volume expansion problem, dense MAS ceramics are normally prepared following a double stage-firing process [14,15]. In this process, the raw materials mixtures are initially calcined at around 1500 °C to obtain spinel phase contents >85%, followed by re-grinding the calcined powder, re-compaction and re-firing at >1650 °C to obtain the desired density. The involvement of two consecutive

* Corresponding author. Tel.: +91 40 24441075/76; fax: +91 40 24442699.
E-mail addresses: ibram_ganesh@yahoo.com, ibramganesh@arci.res.in (I. Ganesh).

0272-8842/$36.00
doi:10.1016/j.ceramint.2009.09.002

Table 1
Compositions of precursor mixtures and characteristics of calcined (1400 °C, 1 h) MAS ground powders.

Sample[a]	Composition (wt.%)		Crystalline phases formed (1400 °C, 1 h) (%)	Average particle size (μm)	Expected MAS phase upon complete reaction (%)	BET surface area (m^2/g)
	Al_2O_3	MgO				
MAS-0	71.8	28.2	$MgAl_2O_4$ (98.1), MgO (1.9)	1.92	100	3.88
MAS-5	70.3	29.7	$MgAl_2O_4$ (89.2), Al_2O_3 (1.92) and MgO (8.88)	2.29	93.04	5.22

[a] MAS-0 and MAS-5 stand for stoichiometric $MgAl_2O_4$ spinel, and a 5 wt.% alumina deficient composition, respectively.

high temperature firing cycles significantly increases the production costs of dense MAS ceramics. Moreover, the preparation of MAS components for certain important strategic applications such as infrared domes and radomes is also quite expensive [16–19]. At present, MAS components for infrared dome and radome applications are being fabricated by hot isostatic pressing (~1500 °C and 200–400 MPa pressure) followed by extensive and expensive machining to obtain the desired final shape [16,17]. Near-net shape forming techniques like aqueous gelcasting can reduce the processing cost of MAS infrared domes and radomes very significantly as post-sintering machining operations can be minimized or even eliminated [19–21]. However, the basic nature of MAS powder and its promptness to react with water make the aqueous gelcasting routes troublesome [5,21]. In our lab, a process for passivating MAS powder against hydrolysis has been successfully developed [22]. The surface passivated MAS powder could then be dispersed in water to obtain stable slurries with 45 vol.% solids loading, suitable for colloidal processing. Nevertheless, the literature information on the relationship between the microstructure and mechanical properties of aqueous processed MAS ceramics is still scarce.

The present work aims at fulfilling the above mentioned gaps. A stoichiometric $MgAl_2O_4$ spinel and a powder with 2.017 wt.% excess of MgO formed by the calcination of alumina and calcined caustic magnesia mixture compacts at 1400 °C for 1 h were fine ground, surface passivated against hydrolysis and dispersed in aqueous medium. The as obtained slurries were consolidated by different processing techniques: slip casting (SC), hydrolysis assisted solidification (HAS) and hydrolysis induced aqueous gelcasting (GCHAS). For comparison purposes, dense MAS ceramics were also fabricated by gelcasting (GC), temperature induced gelation (TIG) and conventional dry-powder pressing (DP) routes. Differently consolidated MAS bodies were sintered for 1 h at 1650 °C and then thoroughly characterized for various properties to establish the effects of processing route on microstructure evolution and its influence on the sintered and mechanical properties of MAS ceramics.

2. Experimental procedure

2.1. MAS powder synthesis and processing

Alumina (CT-3000SG, Alcoa-Chemie GmbH, Ludwigshafen, Germany, average particle size = 1.84 μm, BET SSA ~4 m^2/g, consisting of corundum phase, ICDD File No: 00-46-1212) and calcined caustic magnesia (José M. Vaz Pereira, S.A., Porto, Portugal, average particle/agglomerate size = 5.63 μm, BET SSA ~15 m^2/g, consisting of periclase phase, ICDD File No: 00-45-946) were mixed in two different proportions (Table 1): (i) a stoichiometric mixture (71.8% Al_2O_3 + 28.2% MgO) termed MAS-0; (ii) a 5 wt.% alumina deficient mixture (70.3% Al_2O_3 + 29.7% MgO) termed MAS-5. The powders mixtures were dispersed in an azeotropic mixture of 60 vol.% methyl ethyl ketone (MEK) and 40 vol.% ethanol (E) with the help of Hypermer KD1 as dispersant to achieve about 40 vol.% solids loading in the slurries. The resultant slurries were de-agglomerated for 24 h in polypropylene bottles using alumina balls and a powder to balls weight ratio of 1:3 and were consolidated by temperature induced gelation (TIG) technique [24]. The dried consolidates were then calcined in an electrically heated open-air muffle furnace for 1 h at 1400 °C to obtain MAS powders [14,15]. These calcined powders were crushed, ground in an hammer mill (Retsch GmbH, model SK1, Haan, Germany) and then planetary ball milled (Retsch GmbH, PM400, Haan, Germany) for 3 h at 200 rpm in an absolute ethanol. The solids loading in the slurry maintained was 30 vol.% and the powder to balls weight ratio of 1:3.

The ground MAS-0 and MAS-5 powders were passivated against hydrolysis according to a surface treatment procedure reported elsewhere [22]. In a typical experiment, 245 g of MAS-0 or MAS-5 was suspended in an absolute ethanol to obtain 250 mL of a 30 vol.% suspension in a 500 mL volume three-neck round-bottom (RB) flask. The RB flask was fitted with an equalization funnel and a valve to pass dry nitrogen gas, and was placed into a thermostatic oil bath (150 mm diameter and 80 mm height Pyrex glass dish, Thermol-100, Biolabs, India, −50 to +250 °C). In a separate experiment, 2 g of aluminium dihydrogen phosphate, $Al(H_2PO_4)_3$ (assay ≥97.0%, Fluka, Seelze, Germany) was digested in 5 mL of hot orthophosphoric acid, H_3PO_4 (85% assay, AR grade, Qualigens, Mumbai, India) [23]. This solution was then mixed with 50 mL of ethanol and added drop-by-drop to the above alcohol-based MAS suspension with the help of an equalization funnel. The RB contents were then refluxed for 24 h under a N_2 flow rate of 100 mL/min and magnetic stirring (5MLH-DX, Remi, India). The treated $MgAl_2O_4$ spinel slurries were filtered off and washed with fresh ethanol several times in order to remove the excess of H_3PO_4 and $Al(H_2PO_4)_3$ not bound to the powders' surface.

The compositions and characteristics of MAS slurries prepared for the various processing routes and the setting times are reported in Table 2. Different codes were given to each processing route: GC—gelcasting; SC—slip casting;

Table 2
Characteristics of MAS slurries.

Sample[a]	Raw materials (wt.%)	Slurry medium[b]	Slurry viscosity at $\dot{\gamma} = 230\,s^{-1}$ (mPa s)	Setting time[c] (min)
GC-45	T-MAS-0 (100)	NVPNCPM	251	19 (30)
SC-45	T-MAS-0 (100)	Distilled water	242	30
HAS-5-45	T-MAS-5 (95.9) and AlN (4.1)	Distilled water	214	~1440
GCHAS-5-45	T-MAS-5 (95.9) and AlN (4.1)	NVPNCPM	146	8.214 (15)
TIG-45	MAS-0 (100)	60%MEK + 40%E	–	~1440
DP	T-MAS-0 (100)	Freeze dried T-MAS-0 granules compacted uni-axially in a metal die under 200 MPa		

[a] GC—aqueous gelcasting; SC—aqueous slip casting; HAS—hydrolysis assisted solidification; GCHAS—hydrolysis induced aqueous gelcasting; TIG—temperature induced gelation; DP—dry-powder pressing of freeze dried granules. The numbers 0 and 5 in the sample codes stand for stoichiometric $MgAl_2O_4$ spinel, and a 5 wt.% alumina deficient composition, respectively. The number 45 stands for the volume fraction of solids in the slurries. In the T-MAS-0 and T-MAS-5 codes, T stands for surface treated MAS powders.

[b] NVPNCPM is a 20 wt.% solution of methacrylamide, methylenebisacrylamide and n-vinylpyrrolidone in a 3:1:3 weight ratio in de-ionized water; MEK-methyl ethyl ketone, E-ethanol.

[c] Setting occurred at room temperature, except for TIG-45 (−5 °C). Setting time is defined as the time corresponding to the crossover point ($G' = G''$, please see experimental section for details). The values given in brackets represent the shortest time at which samples could be un-moulded.

HAS—hydrolysis assisted solidification; GCHAS—hydrolysis induced aqueous gelcasting; TIG—temperature induced gelation; DP—dry-powder pressing of freeze dried granules made from aqueous MAS slurries. The number 45 stands for the volume fraction of solids in the slurries. In the case of SC and DP processes, T-MAS-0 powder, and in the case of HAS, T-MAS-5 powder were dispersed in double distilled water by adding 25 wt.% TMAH and Duramax D-3005 aqueous solutions at the ratios of 35 and 30 μL/g of powder, respectively. The dispersed powders were de-agglomerated by ball milling for 24 h in polypropylene bottles using alumina balls with the charge to balls weight ratio of 1:3. The as obtained slurries were sieved (through 150 BSS mesh) and then degassed for 5 min by vacuum pumping. The resultant slurries were directly cast in plaster moulds to obtain slip cast (SC-45) samples or granulated by freeze drying to prepare green samples (30 mm diameter, 8 mm height) by uni-axial DP (200 MPa) [22]. In the case of HAS, 4.1 wt.% AlN on powder basis, was added to 24 h ball milled T-MAS-5 slurry and the milling process continued for further 2 h. The resultant slurry was cast in split-type non-porous aluminium moulds (60 mm × 30 mm × 30 mm) and allowed to consolidate by HAS under ambient conditions [25,26].

The GC-45 and GCHAS-5-45 slurries (Table 2) were prepared by dispersing the surface treated MAS powders (T-MAS-0 and T-MAS-5) in a 20 wt.% premix (NVPNCPM: n-vinylpyrrolidone non-conventional premix) solution in double distilled water of methacrylamide (MAM), methylenebisacrylamide (MBAM) and n-vinylpyrrolidone (NVP) in the ratio of 3:1:3. Aqueous solutions of 25 wt.% tetramethylammonium hydroxide (TMAH) and Duramax D-3005 were added at the ratios of 35 and 30 μL/g of powder, respectively, as dispersing agents. De-agglomeration was performed for 24 h in polypropylene bottles containing alumina balls (12 mm diameter) using a roller mill and a powder to balls weight ratio of 1:3. In the case of GCHAS-5-45, 4.1 wt.% AlN on powder basis, was added to the T-MAS-5 slurry ball milled for 24 h in a 20 wt.% solution of methacrylamide, methylenebisacrylamide and n-vinylpyrrolidone (NVPNCPM) and the milling process continued for further 2 h. These slurries were sieved (through 150 BSS mesh) and degassed for 5 min by vacuum pumping. After introducing a polymerization initiator (10 wt.% aqueous solution of ammonium per-sulphate, APS) and a catalyst (tetramethylethylenediammine, TEMED) at the ratios of 4 and 2 μL/g of slurry, respectively, both slurries were once again degassed for 2 min prior to casting in non-porous white petroleum jelly coated split-type aluminium moulds (60 mm × 30 mm × 30 mm) and setting allowed under ambient conditions [27,28]. All these consolidated parts were dried under controlled humidity (>90% RH and >90 °C) conditions to avoid cracking and non-uniform shrinkage. For comparison purposes, the un-treated MAS-0 powder was also consolidated by TIG process. For this purpose, the MAS powder was dispersed in an azeotropic mixture of 60 vol.% MEK and 40 vol.% E in the presence of 3 wt.% of Hypermer KD1 as dispersant to achieve 45 vol.% solids loading in the slurry. The resultant slurry was de-agglomerated for 24 h in polypropylene bottles using alumina balls and a powder to balls weight ratio of 1:3. The homogenized slurries were separated from the alumina balls and then transferred to glass beakers and placed in a refrigerator (Whirlpool 310 Deluxe, Whirlpool, Madrid, Spain) at −5 °C to promote consolidation by temperature induced gelation (TIG). The consolidated cakes were evacuated for 24 h under a pressure of 1×10^{-1} Torr using a vacuum pump (98.93 L/min capacity, Model: 949-9315, Varian DS-102; Torino, Italy) at −5 °C. Complete drying was then accomplished in an electric hot-air oven at 90 °C according to a procedure described elsewhere [24]. The fully dried MAS compacts formed by the six different consolidation routes were sintered for 1 h at 1650 °C in open-air atmosphere electrical furnace with $MoSi_2$ heating elements. Heating and cooling rates throughout the entire firing cycle were set at 3 and 5 °C/min, respectively.

2.2. Characterization of powders, slurries and sintered materials

BET surface area of the powders was determined by nitrogen physisorption of liquid nitrogen at −196 °C using a

Gemini Micromeritics analyzer (Model 2360, Micromeritics, Norcross, GA, USA) and assuming a cross section area of N_2 molecule as 0.162 nm^2. Particle size distributions of powders were measured using a particle size analyzer (Coulter LS230, Buckinghamshire, UK). The viscosity of slurries was measured using a rotational Rheometer (Bohlin C-VOR Instruments, Worcestershire, UK). The measuring configuration adopted was a cone and plate (4°, 40 mm, and gap of 150 μm), and flow measurements were conducted between 0.1 and 800 s^{-1}. The same configuration was used to obtain information about the gelation behaviour and the evolution of gel stiffness under dynamic measurements of G' (storage modulus) and G'' (loss modulus) in the linear viscoelastic region for GC-45 and GCHAS-5-45 systems. A time sweep was conducted for 30 min at a constant frequency of 1 Hz. A frequency sweep from 1 to 100 Hz under a constant stress of 100 Pa was performed after 30 min of gel time, i.e., the time corresponding to the crossover point of the G' and G'' curves. XRD patterns were recorded on a Rigaku advanced system (Rigaku, Tokyo, Japan) using diffracted beam mono-chromated Cu Kα (0.15406 nm) radiation source. Crystalline phases were identified by comparison with PDF-4 reference data from International Centre for Diffraction Data (ICDD) [29]. To obtain quantitative information of various phases, the most intense peak of the individual phases was taken into consideration. The peak heights of all the phases were summed up and the percentage concentration of a particular phase was estimated from the ratio of the strongest peak of that phase to the sum of various phases present in a given system. Microstructures of dense MAS ceramics were examined after polishing and etching in boiling H_3PO_4 solution for 5 min were observed by SEM on Hitachi S-4100 equipment (Tokyo, Japan). The grain size and its distribution is measured on a image analyzer using the software (ANSIS Five Digital Imaging Solutions, Olympus soft imaging solutions) supplied along with the equipment. For each sample, about 40–60 grains were considered to create histograms and to find the average grain size. The lines in the grain size distribution plots are the fitting curves according to a Poisson distribution function. Bulk density (BD), apparent porosity (AP), and water absorption (WA) capacity of sintered samples were measured according to Archimedes principle (ASTM C372) using Mettler balance (AG 245, Mettler Toledo, Heuwinkelstrasse, Switzerland) [14,15]. For this purpose, about 10–15 sintered pellets were randomly selected from each batch and crushed into 3–5 mm sized grains and ∼20 g of each sample was taken for measuring the BD, AP and WA properties. For each sample, three measurements of BD, AP, and WA capacity were performed and the results presented are the average (±0.01 error). The mechanical properties evaluated were hardness (H), and flexural strength. Hardness data were collected using a micro-hardness tester (Leitz Wetzler, Germany) by holding a 137° indenter tip for 20 s under a load (P) of 10 kg on the mirror finished surface of the samples. Vickers hardness (H) was calculated as $H = P/2d^2$, d being the half-diagonal indentation impression. About 15–20 indentations were taken per sample for measuring hardness and the presented results are the average of them (±0.01 error). The flexural strength of the green and sintered samples was measured using a 3-point bending test (JIS-R1601). About 8–10 specimens were broke for each case and the estimated error is ±∼3.0 for green samples and ±∼12.0 for sintered samples.

3. Results and discussion

The X-ray diffraction patterns of $MgAl_2O_4$ spinel powders formed by solid-state reaction within the compact mixtures of alumina and calcined caustic magnesia (MAS-0 and MAS-5) at 1400 °C for 1 h are presented in Fig. 1 together with the XRD patterns reported in ICDD files for corundum (ICDD File No: 00-46-1212), periclase (ICDD File No: 00-45-946) and $MgAl_2O_4$ spinel (ICDD File No: 00-21-1152). The main XRD peaks belong to $MgAl_2O_4$ spinel phase. Some minor peaks belonging to corundum and periclase phases could also be identified. As expected, the percentage of $MgAl_2O_4$ spinel phase is higher for MAS-0 (98%) than for MAS-5 (89%) that presents higher amounts of un-reacted alumina and magnesia. These values are close to those expected (100 and 95.5%, respectively) from complete reactions between the raw materials. The extent of the reaction is expected to depend on the degrees of intimacy of powders mixture and compactness achieved in the consolidated bodies [30]. Although the TIG process has the ability to preserve in the green cake the homogeneity achieved in the colloidal slurry, the degree of compactness achieved in this process is somewhat lower in comparison to those achieved in a dry pressing process [7,14,15,30]. Good sintered (1650 °C, 1 h) properties were reported for powder compacts having about 90% $MgAl_2O_4$ spinel phase, an average particle size of 3 μm, and a relative green density of ∼55% [7,30], while a similarly sized powder compacted to the same relative green density but with $MgAl_2O_4$ spinel phase content <80% could not achieve the required degree of densification under the same sintering conditions due to the volume expansion (∼8%) associated with the formation

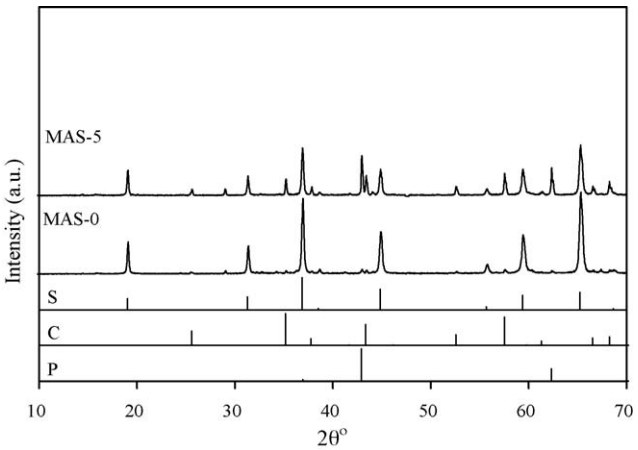

Fig. 1. XRD patterns of $MgAl_2O_4$ spinel powders formed by solid-state reaction (1400 °C, 1 h) from alumina + magnesia: MAS-0, stoichiometric mixture; MAS-5, a 5 wt.% alumina deficient mixture. P, periclase, ICDD File No: 00-45-946; C, corundum, ICDD File No: 00-46-1212; S, spinel, ICDD File No: 00-21-1152.

of $MgAl_2O_4$ spinel phase from un-reacted alumina and magnesia [7,14,15,30].

It was also found that partially (80%) spinelized powders exhibited higher reactivity upon sintering at 1650 °C in comparison with fully spinelized powders [30] that require higher calcination temperatures, which, in turn lead to the formation of hard agglomerates. Based on these findings, the calcination temperature used in the present work was restricted to 1400 °C in order to retain some small amounts of un-reacted alumina and magnesia in the calcined powders, which would react during sintering thereby promoting the densification. According to Wagner mechanism, during the solid-state reaction of corundum and periclase, the $MgAl_2O_4$ spinel phase formation takes place by the counter diffusion of cations through the product layer, while oxygen ions remain at the initial sites [13]. To keep the electro-neutrality, $3Mg^{2+}$ diffuse toward the alumina side and $2Al^{3+}$ diffuse toward the magnesia side to form 3 mol of $MgAl_2O_4$. Therefore, it is of paramount importance to have short diffusion paths between alumina and magnesia particles in the green body by increasing the packing density and by reducing their average sizes.

Attempts to prepare stable and concentrated aqueous suspensions of MAS powders in the presence of several dispersing agents revealed to be unsuccessful [22,23]. Solids loading could never go beyond 30 vol.% and even so, the slurries coagulated within the first 30 min of the de-agglomeration process. It was concluded that the basic nature and hydrolysis of MAS powder were responsible for the dispersing difficulties. Surface passivation of MAS powders according to the procedure described in the experimental part enabled preparing stable suspensions towards hydrolysis and achieving a solids loading of 35 vol.% in absence of any dispersant. The fabrication of thin wall components like radomes, crucibles and domes with near-net shape requires colloidal slurries with a minimum solids loading of about 45 vol.%. A mixture of TMAH (35 μL/g powder) and Duramax D-3005 (30 μL/g powder) revealed to be effective in preparing aqueous suspensions containing 45 vol.% of the surface treated MAS powders (T-MAS-0 and T-MAS-5, or T-MAS-5 + 4.1 wt.% AlN) [22], enabling zeta potential value of ∼45 mV for the T-MAS-0 powder [24]. It has been reported that zeta potential values of $>\pm 40$ mV are required to obtain suitable aqueous slurry for net shape forming of thin wall complex shape components like radomes [31]. Fig. 2 shows a defect free 500 mL capacity crucible consolidated by GCHAS from a slurry containing 45 vol.% of (T-MAS-5 + 4.1 wt.% AlN) in an indigenously made split-type non-porous aluminium mould.

Table 2 reports the composition of the slurries in terms of raw materials and dispersing medium, as well as the viscosity measured at a shear rate of 230 s^{-1}, and setting time. The relatively low viscosity values make the suspensions suitable for net shape fabrication of components [26–28]. The setting times of the GC-45 and GCHAS-5-45 systems upon addition of polymerization initiator (i.e., APS) and catalyst (i.e., TEMED) were relatively short. Slip cast sample (SC-45) could be un-moulded after 30 min, while the bodies consolidated by HAS and TIG (HAS-5-45, TIG-45) took more than 24 h for acquiring the handling strength. These results are quite comparable with those reported for other ceramics consolidated by similar processing techniques [20,25–28].

Fig. 2. A $MgAl_2O_4$ spinel crucible (∼500 mL capacity) consolidated by hydrolysis induced aqueous gelcasting (GCHAS) from a slurry containing 45 vol.% of T-MAS-5 + AlN (4.1 wt.%) powders.

The evolution with time of storage (elastic) modulus (G') and of the loss (viscous) modulus (G'') of GC-45 and GCHAS-5-45 slurries upon addition of polymerization initiator and catalyst is plotted in Fig. 3(a) and (b), respectively. A gradual increase of both elastic and viscous components with increasing time is noticed. The viscous character predominates over the elastic one along a first period that ends at the crossover point where $G' = G''$. The elapsed time up to this point is usually taken as the gelation time [28], beyond which the elastic character of the gelling systems predominates over the viscous one ($G' > G''$) for about 1–2 orders of magnitude (Fig. 3(b)).

The mechanical spectra of GC-45 and GCHAS-5-45 slurries recorded at ambient temperature after about 30 min of gelation are presented in Fig. 4. Due to the large differences in magnitude between G' and G'', the dynamic analysis was restricted to elastic component only. In fact, under the tested conditions, the measurement of G'' is no longer reliable because it depends on the instrumental resolution of the phase lag between sinusoidal stress and strain [28]. Fig. 4 shows that both the curves run almost parallel to the X-axis, a characteristic behaviour of stiff gels. The GCHAS-5-45 system is stiffer than GC-45 due to the synergetic effect of added AlN, the hydrolysis of which is accompanied by consumption of water and the formation of 'cementing' aluminium hydroxides that strengthen the gel [25,26].

Table 3 presents the values of bulk density (BD), relative density (RD), apparent porosity (AP), water absorption (WA) capacity, grain size (minimum, maximum and average), linear shrinkage (LS), hardness and 3-point bending strength of MAS

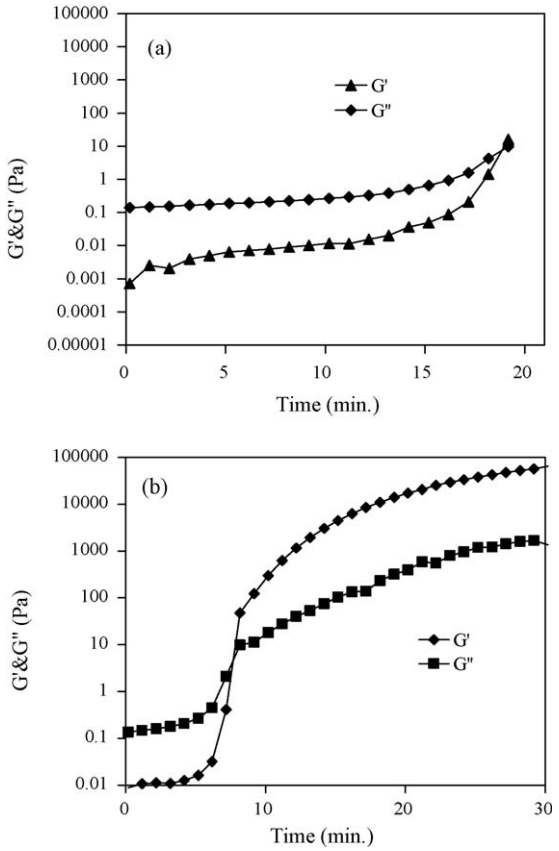

Fig. 3. Evolution of G', G'' with time after adding the polymerization initiator and catalyst to: (a) GC-45 and (b) GCHAS-5-45 slurries. The gelation time is given by the crossover point when $G' = G''$.

ceramics sintered for 1 h at 1650 °C together with their corresponding green (density, strength and linear shrinkage) properties. The relative density values of greens varied from 45.16 to 46.50%. Bodies consolidated by non-liquid removal colloidal processes (HAS-5-45, GCHAS-5-45, GC-45 and TIG-45) were expected to possess lower green densities as the degree of packing is dictated by the solids loading of the slurry and the shrinkage on drying. However, no appreciable density differences were measured between these samples and that

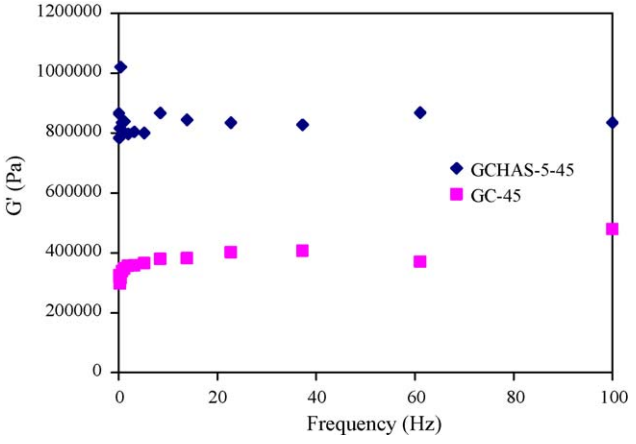

Fig. 4. Frequency dependent elastic modulus of the GC-45 and GCHAS-5-45 systems measured after their respective gelation times.

consolidated by slip casting (SC-45). The presence of 4.1 wt.% AlN, a component less dense (3.26 g/cm^3) than MAS (3.58 g/cm^3), did not negatively affect the green density (GD) of GCHAS-5-45 in comparison to GC-45. Therefore, the lower GD of HAS-5-45 can be attributed to the absence of a fine three-dimensional network formed by the *in situ* polymerization of monomers that creates a higher driving force for shrinkage, which is expected to strengthen the consolidates, as observed. The percentage linear shrinkage (LS) upon setting and drying is inversely related to the GD, as expected. All LS values are in the safety range (<4%) for a successful fabrication of complex-shaped components by near-net shaping routes [27,28].

TIG-45 samples were found to be hard but very fragile not permitting measuring the 3-point bending strength. In fact, no binding mechanism other than chain entanglement of dispersant molecules and mechanical interlocking of particles is involved in the TIG process [24]. In the case of HAS process, the particles are held together by the cementing action of $Al(OH)_3$ formed upon hydrolysis of AlN [25,26]. The sample GCHAS-5-45 is benefited from both strengthening mechanisms offered by gelcasting and HAS processes being the strongest one. Based on green strength, the MAS consolidates can be ordered as: GCHAS-5-45 (21.23 ± 0.42 MPa) > GC-45 (15.64 ± 2.38 MPa) > HAS-5-45 (11.849 ± 1.76 MPa) > SC-45 (7.832 ± 2.16 MPa) > DP (0.245 ± 0.3 MPa). These results clearly suggest GCHAS as the most interesting process for fabricating thin wall MAS components like radomes and domes as it confers a very high green strength to the greens permitting green machining to obtain the desired shape.

Based on sintered density, the MAS ceramics can be arranged as: GC-45 (98.43%) > DP (97.93%) > GCHAS-5-45 (96.92%) > SC-45 (94.89%) > HAS-5-45 (94.07%) > TIG-45 (93.74%). Though having theoretical pore volume fractions in the range of 1.57–6.26%, the values of apparent porosity and water absorption capacity are lower than 1.5 and 1%, respectively, indicating the presence of significant closed porosity fractions. Table 3 reveals that the densification behaviour is strongly influenced by the degree of packing achieved in the green compact. Accordingly, DP, GC-45 and GCHAS-5-45 samples with relatively higher green densities show superior sintered properties. Although the green SC-45 and GC-45 samples exhibit similar degrees of packing, the sintered density of SC-45 is about 3.5% lower. This suggests the occurrence of some particle segregation during the liquid removal due to the clogging effect [32]. The poor densification ability of TIG-45 could be ascribed to its low green density and weak adhesion among the particles reflected in the poor green strength. Oppositely, the intricate 3D network of fine pores derived from the polymerization of organic monomers in GC-45 and GCHAS-5-45, causes the development of high capillary pressures in the pores, enhancing particles packing in the green consolidates, their sintering ability [20] and final mechanical properties. MAS ceramics with ~95% of the theoretical density were considered suitable for several applications [4,7,33,34], qualifying DP, GD and GCHAS as promising processes for their fabrication.

A $MgAl_2O_4$ spinel with a BD of 2.98 g/cm^3, an AP of 16.0%, a Vickers hardness of 340 VHN and an average crystallite size of

Table 3
Properties of green and sintered (1650 °C for 1 h) MAS ceramics.[a].

Sample[b]	Green properties				Sintered properties							Hardness (kg/mm^2)	Flexural strength (MPa)
	GD (g/cm^3)	RD (%)	LS upon drying (%)	Flexural strength (MPa)	BD (g/cm^3)	RD (%)	AP (%)	WA (%)	LS (%)	Grain size (μm)				
										Min.	Max.	Ave.		
GC-45	1.635	45.67	2.878	15 ± 2.38	3.52 ± 0.04	98.43	0.275	0.083	18.249	3.21	15.82	7.08	800 ± 13.05	183 ± 8.4
SC-45	1.623	45.33	–	7 ± 2.16	3.39 ± 0.07	94.89	1.034	0.785	17.683	3.01	12.92	5.73	656 ± 19.30	153 ± 11.0
HAS-5-45	1.617	45.16	2.936	11 ± 1.76	3.36 ± 0.08	94.07	0.132	0.055	17.831	3.73	17.17	8.40	1192 ± 16.51	112 ± 9.4
GCHAS-5-45	1.638	45.75	3.156	21 ± 0.42	3.47 ± 0.05	96.92	0.256	0.076	17.832	3.45	18.27	8.33	1197 ± 19.45	169 ± 11.2
TIG-45	1.627	45.44	3.046	–	3.35 ± 0.06	93.74	1.491	0.438	17.653	3.56	13.94	6.91	1092 ± 34.42	–
DP	1.665	46.50	–	0.25 ± 0.3	3.50 ± 0.03	97.93	0.064	0.018	17.537	3.43	12.8	6.48	811 ± 18.63	173 ± 5.3

[a] GD—green density; RD—relative density; LS—linear shrinkage; BD—bulk density; AP—apparent porosity; WA—water absorption capacity.
[b] GC—aqueous gelcasting; SC—aqueous slip casting; HAS—hydrolysis assisted solidification; GCHAS—hydrolysis induced aqueous gelcasting; TIG—temperature induced gelation; DP—dry pressing of freeze dried granules. The numbers 5 and 45 in the sample codes stand for the 5 wt.% alumina deficient composition, and the volume fraction of solids in the slurries, respectively.

43.6 nm formed upon sintering (for 50 h at 1550 °C in a single-stage reaction sintering process) a stoichiometric mixture of MgO and Al_2O_3 compacted in a 2.5 cm diameter metal die uni-axially under a pressure of 400 MPa exhibited an electrical conductivity of 1.2 S/cm. This material has out performed the carbon electrode in an aluminium metallurgical industry [4]. A stoichiometric $MgAl_2O_4$ spinel formed with a BD of 3.40 g/cm^3, AP of 0.193% and WA capacity of 0.057% upon sintering for 1 h at 1550 °C under the influence of 2.733 wt.% $AlCl_3$, a sintering aid, has improved the slag erosion and penetration resistance of high Al_2O_3 refractory by 58 and 14.5%, respectively, and slag erosion resistance of MgO–C refractory by 48% when 20 wt.% of it was added to the latter bricks and heated to 1650 °C for 2 h in an electrical furnace [7]. A polycrystalline ceramic formed by the sintering of a mixture of stoichiometric $MgAl_2O_4$ spinel powder and an organic fugitive material at 1600 °C for 4 h had a porosity of about 5.5% and exhibited a breakdown dielectric strength of 450 kV/cm [33]. A stoichiometric $MgAl_2O_4$ spinel powder formed upon calcination of reagent grade MgO and Al_2O_4 mass ball milled for 24 h in water using zirconia balls in air at 1500 °C for 3 h was fine ground, added with 6 wt.% PVA, and pressed into disks measuring 12 mm in diameter and 2–6 mm in height and then sintered at 1650 °C in air for 3 h. These sintered polycrystalline ceramics had a grain size of about 5 μm and a porosity of about 1% exhibited a dielectric constant (ε) of 7.8 and a product of quality factor (Q) and frequency (f) of about 82,500 GHz at 14.5–15.7 GHz measured according to the resonator method [34].

Table 3 confirms that the MAS ceramics consolidated by the present colloidal processing routes exhibit better mechanical properties (hardness and 3-point bend strength) in comparison to those prepared by the other shaping techniques. A hardness of 779 kg/mm^2 was reported by Bhaduri and Bhaduri [35] for a nanocrystalline dense MAS consolidated by the non-aqueous slip casting, followed by cold iso-static pressing (CIPing) at 275 MPa for 10 min and then by hot iso-static pressing (HIPing) at 1300 °C for 4 h. The hardness and flexural strength values observed in the present study without using such heavy equipments are therefore comparable to those reported in the literature for MAS ceramics [36].

The linear shrinkage upon sintering of these MAS ceramics did not exceed 18.5%, being within the safety range for net shape fabrication of thin wall components devoid of any defect [27]. All the MAS ceramics exhibited (not shown here) diffraction peaks only due to MAS phase (ICDD File No: 00-21-1152) upon sintering for 1 h at 1650 °C. Such results were expected even for the HAS-5-45 and GCHAS-5-45 systems, which designed in such a way that after complete hydrolysis of AlN (4.1 wt.%) the stoichiometric MAS composition should be attained. According to the binary MgO–Al_2O_3 phase diagram, $MgAl_2O_4$ is the only phase formed at temperatures up to 1600 °C [13]. At this temperature, the solid solubility of MgO and Al_2O_3 in the spinel is 2 and 6%, respectively. On increasing the firing temperature to 1700 °C, the solubility in the spinel increases to 3.0 and 10.0%, respectively. This solid solubility helps to explain why minor phases could not be identified by XRD in none of the samples sintered for 1 h at 1650 °C.

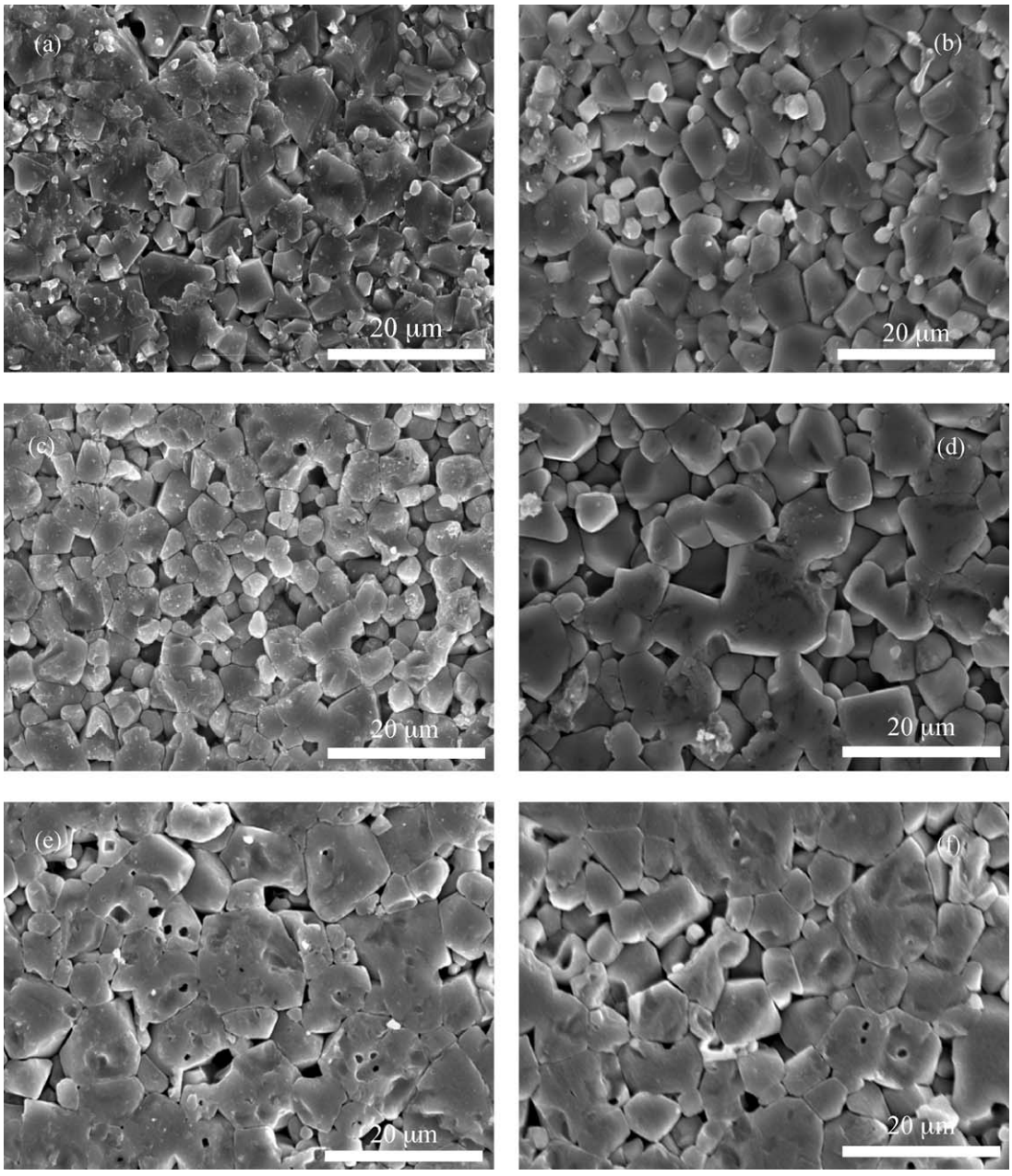

Fig. 5. SEM micrographs of sintered (1650 °C, 1 h) ceramics consolidated by (a) DP, (b) TIG-45, (c) SC-45, (d) GC-45, (e) HAS-5-45, and (f) GCHAS-5-45.

The SEM micrographs of DP, TIG-45, SC-45, GC-45, HAS-5-45 and GCHAS-5-45 samples sintered for 1 h at 1650 °C are presented in Fig. 5(a)–(f), respectively, and their corresponding grain size histograms and the average grain size (AGS) in Fig. 6. The lines in the grain size distribution plots are the fitting curves according to a Poisson distribution function. It can be seen from Fig. 5 that all the samples consist of equi-axed grains (in the size range of 3.01–18.27 μm, Table 3) packed with varied closeness. In general, these microstructures reveal the presence of both intra- and inter-grain porosities. In accordance with the findings of Archimedes principle, the microstructures reveal considerable amount of closed porosity (intra-grain porosity), what is seen very clearly in the microstructures of HAS-5-45 (Fig. 5(e)) and GCHAS-5-45 (Fig. 5(f)), which had AlN (4.1 wt.%) in their starting slurries. Furthermore, the sintered GC-45, DP and GCHAS-5-45 samples seem to possess more densely packed grains then the others. Among the six samples, the HAS-5-45 and GCHAS-5-45 consist of an apparent higher fraction of larger grains, which could be responsible for their measured higher hardness. Nevertheless, the SEM micrographs of these ceramics are quite comparable with those reported for MAS ceramics in the literature [3,14,15,30,35,36].

The grain size histograms reveal that the DP (3.43–12.8 μm and 6.48 μm) and SC-45 (3.01–12.92 μm and 5.73 μm) possess narrow grain size distributions and lower average grain sizes, whereas, the HAS-5-45 (3.73–17.17 μm and 8.40 μm) and GCHAS-5-45 (3.45–18.27 μm and 8.33 μm) contain relatively wide grain size distributions and large average grain sizes. The GC-45 and TIG-45 contain intermediate grain size distributions

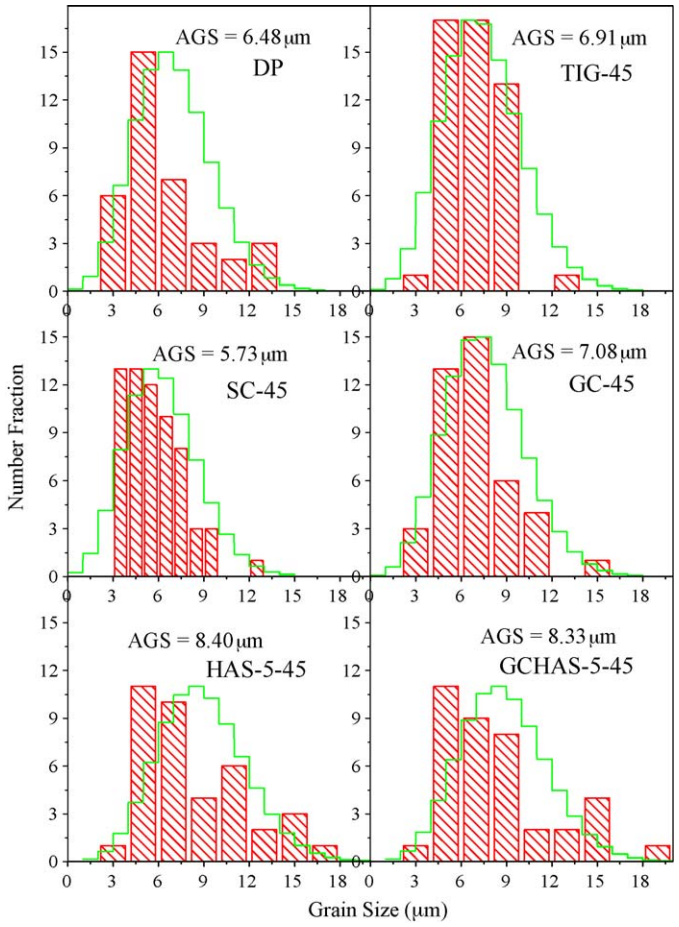

Fig. 6. The grain size histogram and the average grain size of DP, TIG-45, SC-45, GC-45, HAS-5-45, and GCHAS-5-45 ceramics sintered for 1 h at 1650 °C measured from SEM micrographs shown in Fig. 5 using an image analyzer. The lines in the grain size distribution plots are the fitting curves according to a Poisson distribution function (AGS stands for average grain size).

and average grain sizes (Table 3 and Fig. 6). The flexural strength of these ceramics appears to depend more on the degree of the densification achieved upon sintering in comparison to the grain size and its distribution. Nevertheless, the measured grain size and grain size distribution data are similar to those of MAS ceramics consolidated by other techniques and sintered [33,34].

4. Conclusions

The following conclusions can be drawn from this study:

1. The magnesium aluminate spinel (MAS) powders with more than 89% spinel phase could be prepared by calcining at 1400 °C for 1 h the mixtures of alumina and calcined caustic magnesia consolidated by the temperature induced gelation (TIG) process.
2. The surface of the MAS powders was passivated against hydrolysis by coating with phosphate species [H_3PO_4 and $Al(H_2PO_4)_3$] dissolved in ethanol and kept at 80 °C for 24 h.
3. The surface passivated MAS powders could be dispersed in aqueous media to prepare stable slurries with 45 vol.% solids loading using suitable amounts of TMAH and Duramax D-3005 as dispersing agents.
4. Dense MAS ceramics with 94–98% of theoretical density could be obtained by sintering for 1 h at 1650 °C green bodies consolidated by gelcasting, slip casting, hydrolysis assisted solidification, and hydrolysis induced aqueous gelcasting.
5. Among the various colloidal processing routes, the hydrolysis induced aqueous gelcasting was found to be the most promising process for fabricating near-net shape thin wall MAS ceramics.

Acknowledgements

IG thanks SERC-DST (Government of India) for the awarded BOYSCAST fellowship (SR/BY/E-04/06). S.M. Olhero wishes to thank to Foundation for Science and Technology (FCT) of Portugal for the financial support under the grant SFRH/BPD/27013/2006. The financial support of CICECO is also acknowledged. GJR thanks Director, ARCI for awarding senior ARCI fellowship (SAF). Authors wish to thank the distinguished reviewer for his valuable and constructive comments that have improved the quality of the paper.

References

[1] A. LaReoche, K. Rzenburg, J. Voyles, L. Fehrenbacher, G. Gilde, An economic comparison of hot pressing vs. pressureless sintering for transparent spinel armor, in: Lisa Prokuart Franks (Ed.), Advances in Ceramic Armor-IV, Ceramic Engineering and Science Proceedings, vol. 29, no. 6, in: Tatsuki Ohji, Andrew Wereszczak (Eds.), The American Ceramic Society, A John Wiley and Sons, Inc., 2008, pp. 55–62.
[2] J.L. Sepulveda, R.O. Loutfy, S. Chang, Defect free spinel ceramics of high strength and high transparency, in: Lisa Prokuart Franks (Ed.), Advances in Ceramic Armor-IV, Ceramic Engineering and Science Proceedings, vol. 29, no. 6, in: Tatsuki Ohji, Andrew Wereszczak (Eds.), the American Ceramic Society, A John Wiley and Sons, Inc., 2008, pp. 75–88.
[3] L. Ji-Guang, T. Ikegami, L. Jong-Heum, T. Mori, Fabrication of translucent magnesium aluminate spinel ceramics, J. Am. Ceram. Soc. 83 (11) (2000) 2866–2868.
[4] S. Angappan, L.J. Berchmans, C.O. Augustin, Sintering behaviour of $MgAl_2O_4$—a prospective anode material, Mater. Lett. 58 (2004) 2283–2289.
[5] Y. Shimizu, H. Arai, T. Seiyama, Theoretical studies on the impedance-humidity characteristics of ceramic humidity sensors, Sens. Actuators 7 (1985) 11–22.
[6] M. O'Driscoll, Fused spinel—monolithics market future, IM Fused Minerals Review Special Issue (1997) 36–46.
[7] I. Ganesh, S. Bhattacharjee, B.P. Saha, R. Johnson, K. Rajeshwari, R. Sengupta, M.V. Ramanarao, Y.R. Mahajan, An efficient $MgAl_2O_4$ spinel additive for improved slag erosion and penetration resistance of high-Al_2O_3 and MgO–C refractories, Ceram. Int. 28 (2002) 245–253.
[8] C. Baudin, R. Martinez, P. Pena, High-temperature mechanical behavior of stoichiometric magnesium spinel, J. Am. Ceram. Soc. 78 (7) (1995) 857–1862.
[9] P. Hing, Fabrication of translucent magnesium aluminate spinel and its compatibility in sodium vapour, J. Mater. Sci. 11 (1976) 1919–1926.
[10] K.E. Green, J.L. Hastert, D.W. Roy, Polycrystalline $MgAl_2O_4$ spinel—a broad band optical material for offensive environments, in: Window & Dome Technologies and Material, Proc. Soc. Photo-Opt. Instrum. Eng., A90-34551, 1989, pp. 14–74.

[11] M.A. Sainz, A. Mazzoni, E. Aglietti, A. Caballero, Thermo-chemical formation and stability of spinel under strongly reducing conditions, in: Proceedings of the UNITESR'95, 1995, pp. 387–392.
[12] J.H. Belding, E.A. Letzgus, Process for producing magnesium aluminate spinel, U.S. Patent No. 3,950,504 (April 13, 1976).
[13] Z.E. Nakagawa, N. Enomoto, I.S. Yi, K. Asano, Effect of corundum/periclase sizes on the expansion behavior during synthesis of spinel, in: Proceedings of the UNITESR'95, Congress, Tokyo, (1995), pp. 379–386.
[14] I. Ganesh, K.A. Teja, N. Thiyagarajan, R. Johnson, B.M. Reddy, Formation and densification behavior of magnesium aluminate spinel: the influence of CaO and moisture in the precursors, J. Am. Ceram. Soc. 88 (10) (2005) 2752–2761.
[15] I. Ganesh, S.M. Olhero, A.H. Rebelo, J.M.F. Ferreira, Formation and densification behaviour of $MgAl_2O_4$ spinel: the influence of processing parameters, J. Am. Ceram. Soc. 91 (6) (2008) 1905–1911.
[16] D.W. Roy, S.H. Evans, Correlation of strength and processing variables for optical-quality spinel, in: G.W. Wilkerson (Ed.), Passive Materials for Optical Elements II, Proc. Soc. Photo-Opt. Instrum. Eng., 1993, p. 2018.
[17] D.W. Roy, G.G. Martin, Advances in spinel optical quality, size/shape capacity, and applications, in: Paul Klocek (Ed.), Window & Dome Technologies and Materials III, Proc. Soc. Photo-Opt. Instrum. Eng., 1992, p. 1760.
[18] K. Rozenburg, I.E. Reimanis, H.-J. Kleebe, R.L. Cook, Sintering kinetics of $MgAl_2O_4$ spinel doped with LiF, J. Am. Ceram. Soc. 91 (2) (2008) 444–450.
[19] P. Kumar, K.H. Sandhage, Near net-shaped magnesium aluminate spinel by the oxidation of solid magnesium-bearing precursors, in: TMS Outstanding Student Paper Contest Winner-1998, Graduate Division, Department of Materials Science and Engineering, The Ohio State University, Columbus, OH, 1998.
[20] M.A. Janney, S.D. Nunn, C.A. Walls, O.O. Omatete, R.B. Ogle, G.H. Kirby, A.D. McMillan, Gelcasting, in: M.N. Rahman (Ed.), The Handbook of Ceramic Engineering, Marcel Dekker, New York, 1998, pp. 1–15 (references there in).
[21] L. Kaiqi, P. Wei, F. Zhengkun, L. Yongfeng, W. Bingjun, Gelcasting of alumina-spinel refractories, Key Eng. Mater. 368–372 (2008) 1149–1151.
[22] I. Ganesh, S.M. Olhero, P.M.C. Torres, J.M.F. Ferreira, Gelcasting of $MgAl_2O_4$ spinel powder, J. Am. Ceram. Soc. 92 (2) (2009) 350–357.
[23] I. Ganesh, S.M. Olhero, A.A. Branca, M.R. Correia, G. Sundararajan, J.M.F. Ferreira, Chemisorption of phosphoric acid and surface characterization of as passivated AlN powder against hydrolysis, Langmuir 24 (10) (2008) 5359–5365.
[24] L. Bergström, Method for forming ceramic powders by temperature induced flocculation, U.S. Patent 5,340,532 (August 23, 1994).
[25] T. Kosmac, S. Novak, M. Sajko, Hydrolysis-assisted solidification (HAS): a new setting concept for ceramic net-shaping, J. Eur. Ceram. Soc. 17 (1997) 427–432.
[26] I. Ganesh, N. Thiyagarajan, D.C. Jana, P. Barik, G. Sundararajan, J.M.F. Ferreira, Dense β-SiAlONs consolidated by a modified hydrolysis assisted solidification route, J. Eur. Ceram. Soc. 28 (4) (2008) 879–885.
[27] I. Ganesh, Near-net shape β-$Si_4Al_2O_2N_6$ parts by hydrolysis induced aqueous gelcasting process, Int. J. Appl. Ceram. Technol. 6 (1) (2009) 89–101.
[28] I. Ganesh, S.M. Olhero, P.M.C. Torres, F.J. Alves, J.M.F. Ferreira, Hydrolysis induced aqueous gelcasting for near-net shape forming of ZTA ceramic composites, J. Eur. Ceram. Soc. 29 (2009) 1393–1401.
[29] B.D. Cullity, Elements of XRD, 2nd ed., Addison-Wesley, Reading, MA, 1978.
[30] I. Ganesh, S. Bhattacharjee, B.P. Saha, R. Johnson, Y.R. Mahajan, A new sintering aid for magnesium aluminate spinel, Ceram. Int. 27 (2001) 773–779.
[31] J.A. Lewis, Colloidal processing of ceramics, J. Am. Ceram. Soc. 83 (10) (2000) 2341–2359.
[32] J.M.F. Ferreira, Role of the clogging effect in the slip casting process, J. Eur. Ceram. Soc. 18 (1998) 1161–1169.
[33] A.S. Rupaal, J.E. Garnier, J.L. Bates, Dielectric breakdown of porous $MgAl_2O_4$, J. Am. Ceram. Soc. 64 (7) (1981) (C-100-C-101).
[34] C.W. Zheng, S.Y. Wu, X.M. Chen, K.X. Song, Modification of $MgAl_2O_4$ microwave dielectric ceramics by Zn substitution, J. Am. Ceram. Soc. 90 (5) (2007) 1483–1486.
[35] S. Bhaduri, S.B. Bhaduri, Microstructural and mechanical properties of nanocrystalline spinel and related composites, Ceram. Int. 28 (2002) 153–158.
[36] K.W. White, G.P. Kelkar, Fracture mechanisms of a coarse-grained, transparent $MgAl_2O_4$ at elevated temperatures, J. Am. Ceram. Soc. 75 (12) (1992) 3440–3444.